J Nanopart Res (2023) 25:165
https://doi.org/10.1007/s11051-023-05808-0

RESEARCH PAPER

Aptamer- and antibody-conjugated gold nanobipyramids—a study on cytotoxicity towards breast cancer cell lines

Bankuru Navyatha · Seema Nara

Received: 28 September 2022 / Accepted: 17 July 2023 / Published online: 31 July 2023

Abstract Specifically targeted gold nanobipyramids (GNBs) hold great potential as photothermal therapeutic agent apart from various other applications such as contrast agents in diagnostic imaging techniques, biosensors, drug delivery, and hence their cytotoxicity need to be determined. Further, the efficiency of specifically targeted therapeutic delivery depends on various factors such as expression levels of target protein, targeting moiety, route of administration, and location of tissue. Hence, it is desirable to understand the efficiency of targeting moieties such as aptamers and antibodies in specifically targeting their target protein and their effect on cytotoxicity. Studies comparing the targeting efficiency of aptamer- and antibody-conjugated gold nanobipyramids on their cytotoxicity; targeting ability and photothermal effect are very scarce. In this perspective, present study investigates the photothermal properties of gold nanobipyramids and compares the effect of targeting moiety against MUC1 protein on cell cytotoxicity and thermal effect on MCF7 cell lines and HCT116 cell lines. Transmission electron microscopy (TEM) micrographs represented that the synthesized gold nanostructures were of bipyramidal shape with an average length of 71.73 nm and width of 27.7 nm. The results showed that conjugation with aptamer had greatly reduced the cytotoxicity of nanobipyramids on both the cell lines compared to antibody conjugation. In vitro photoablation studies revealed that aptamer-conjugated nanobipyramids were more efficient in specifically photoablating MCF7 cell lines w.r.t HCT116 cell lines in comparison to antibody-conjugated nanobipyramids which were consistent with cellular uptake studies.

Keywords Gold nanobipyramids · Photothermal therapy · Aptamer · Antibody · Cytotoxicity · Biocompatibility

Introduction

Gold nanobipyramids are evolving as promising candidates because of their diverse biomedical applications in in vitro and in vivo imaging and diagnostics, spectroscopy, photocatalysis, photothermal therapy, and drug delivery applications. They offer unique plasmonic properties which contribute to high absorption and scattering coefficient, efficient light to heat conversion, and high photostability [1–3]. Gold nanobipyramids with broad base and sharp tips find advantage in biomedical photonic applications because of their narrow plasmonic peaks,

Supplementary Information The online version contains supplementary material available at https://doi.org/10.1007/s11051-023-05808-0.

B. Navyatha · S. Nara (✉)
Department of Biotechnology, Motilal Nehru National Institute of Technology Allahabad, Prayagraj 211004, U.P, India
e-mail: seemanara@mnnit.ac.in; seemanara@gmail.com

flexible tuning of their LSPR towards NIR window, and strong local electric field enhancements. The presence of two sharp edges endows them to absorb light efficiently in comparison to other popularly used gold nanostructures like nanospheres and nanorods. These possess several folds higher two-photon action cross section than that of organic fluorophores which assists as energy donors in photothermal and photodynamic therapies [4–6]. Further, tunable absorption wavelengths, fascinating shape homogeneity, and high chemical stability of nanobipyramids in comparison to other gold nanostructures make them better probes for nanotheranostics. For example, Feng et al. developed folic acid-conjugated gold nanobipyramid-based theranostic probe for surface-enhanced Raman scattering-mediated phototherapy of breast cancer cells [7]. Similarly, Li and group designed indocyanine green-conjugated mesoporous silica-coated gold nanobipyramids as light responsive nanotheranostic probe for dual imaging (fluorescence and photoacoustic imaging)-based PTT [8]. The unique properties of nanobipyramids and their applications have been recently reviewed [9]. To increase the applicability of any nanostructure for cancer targeting and therapy, detailed investigations on their cytotoxicity and other properties like photothermal efficiency are needed. For gold nanobipyramids, very few studies have reported their cytotoxicity and application as photothermal and contrast agents in targeting cancer due to limitations of their preparation and modifications [7, 10, 11]. Secondly, to increase the efficiency of tumor targeting, surface modifications of nanostructures are done with specific antibodies or aptamers against tumor antigens [12]. However, the ssDNA aptamer and antibody are entirely different molecules, and the effect of surface modification of nanostructure with these two entities could vary. Hence, this work was undertaken to investigate the cytotoxicity of nanobipyramids and to systematically assess the effect of modifying GNB surface with target specific aptamer and antibody. Further, the impact of surface modification on GNB toxicity and photothermal efficiency was also investigated.

MUC1 protein is a glycoprotein, mucin family member which is overexpressed on the surface of almost all tumor cells and extensively targeted protein for site specific delivery of therapeutic molecules. Hence, it was decided to target MUC1 protein on MCF-7 breast cancer cell lines which overexpresses it on the surface. Recently, Qiao and group [13] have developed and demonstrated a strategy based on MUC1 aptamer-conjugated gold nanobipyramids modified with fluorescent polymer for real-time monitoring of temperature change during PTT and its effect on MCF7 cells. The study showed that MUC1 aptamer conjugation enhanced the fluorescent intensity in MCF7 cells and also the specificity compared to COS-7 cells. However, there is a relative dearth of literature on the studies comparing the efficiency of targeting moiety for delivering nanobipyramids as photothermal agent and their effect on cytotoxicity of nanobipyramids. Such studies are required to have an insight on the therapeutic abilities of nanobipyramids. Thus, the present study was undertaken to fill this knowledge gap by investigating the potential of gold nanobipyramids as PTT agents and the effect of surface modi0fication of nanobipyramids on cancer cell killing and photothermal efficiency.

Materials and methods

Materials

All reagents and chemicals used were of analytical grade or HPLC grade. All reagents and chemicals used for cell culture were of cell culture grade. Gold (III) chloride hydrate, sodium borohydride ($NaBH_4$), cetyltrimethyl ammonium chloride (CTAC) solution, cysteamine dihydrochloride, and polyethylene glycol methyl ether thiol (mPEG-SH) of molecular weight 6000 were purchased from Sigma-Aldrich, India. Cetyltrimethyl ammonium bromide (CTAB), silver nitrate ($AgNO_3$), 8-hydroxyquinoline (HQ), Tween 20, Triton X-100, and sodium hydroxide (NaOH) were purchased from Sisco Research Laboratories Pvt. Ltd., India. RPMI-140, fetal bovine serum, trypsin, 3-(4,5-dimethylthiazol-2-yl)-2,5-diphenyltetrazolium bromide (MTT) reagent, and sucrose were purchased from HiMedia Laboratories Pvt. Ltd., India. The cell lines used in the study were procured from the National Centre for Cell Science, Pune, India. Capture oligonucleotide (5′-SH-GCCTGTTGT GAGCCTCCTGTCGAA-3′) and MUC1 specific aptamer with 5′ modification (5′-Alexa488-GGGAGA CAAGAATAAACGCTCAAGCAGTTGATCCTT TGGATACCCTGGTTCGACAGGAGGCTCACA ACAGGC-3′) [14] MUC1 aptamer was synthesized

from Eurofins Genomics India Pvt. Ltd., India. Alexa-480-tagged anti-MUC1 antibody was purchased from Novus Biologicals (India).

Synthesis of gold nanobipyramids and their PEGylation

In the present study, the synthesis of gold nanobipyramids was carried out by following CTAC-directed, seed-mediated two-step synthesis method. This method involves synthesis of CTAC seed solution and growth of seed mediated by dual surfactant (CTAC and CTAB) and low potential reducing agent 8-hydroxyquinoline.

Synthesis of CTAC seed solution

To a clean dry flask placed on magnetic stirrer, 486 µL of 25% CTAC solution was added, and the solution was volumized to 4 mL to obtain the final concentration of 95 mM. After a gentle stir, 4 mL of 0.5 mM $HAuCl_4$ solution was added, and the stirring was continued for 20–30 s at 20 °C. To this mixture, 72 µL of 250 mM nitric acid was added, and the stirring was increased to 1000 rpm. After stirring for 20 s, 100 µL of reducing solution (equimolar quantity (50 mM) of $NaBH_4$ and NaOH) was added resulting in the formation of brownish color solution. The solution was stirred vigorously (1000 rpm) for 1 min. Now, 16 µL of 1 M trisodium citrate was added and stirred gently. Finally, the flask was placed in a water bath preheated at 85 °C for 1 h to promote aging. After aging, the seed solution was cooled to room temperature naturally.

Synthesis of growth solution

Gold nanobipyramids were synthesized using dual surfactant which involves both CTAB and CTAC as surfactants for directing the growth and stabilization. For this, firstly, the surfactant mixture was prepared by mixing 6 mM CTAB and 140 mM CTAC and volumized to 4 mL. To this 4 mL surfactant mixture, 40 µL of 25 mM $HAuCl_4$ was added and placed on magnetic stirrer under gentle stirring. Twelve microliters of $AgNO_3$ was added, and the stirring was continued for another few seconds. Forty microliters of 0.4 M 8-HQ was added to reduce the gold salt resulting in the transformation of dark yellow solution to pale yellow color solution. After stirring the solution for 1 min, 40 µL of seed CTAC seed solution was added which acts as nucleating centers for the growth of gold nanobipyramids. The flask was placed in a water bath at 45 °C for 15 min. Later on, 30 µL of 0.4 M 8-HQ was added again and placed in a water bath at 45 °C for 90 min for further aging of gold nanobipyramids. After aging, gold nanobipyramids were harvested by centrifuging the solution at 8000 rpm for 10 min and washed with Milli-Q.

Surface modification with thiolated polyethylene glycol (mPEG-SH)

The surface modification of as-synthesized gold nanobipyramids with $mPEG_{6000}$-SH was carried out in 2 mM sodium carbonate buffer. Briefly, to the harvested pellet of gold nanobipyramids, 475 µL of sodium carbonate buffer and 25 µL of 2 mM mPEG-SH solution were added. The above mixture was placed on a shaker at 180 rpm, room temperature for 24 h. After the incubation time, the unbound PEG molecules were removed by spinning at 8000 rpm for 10 min, and the final pellet was dissolved in 1X phosphate buffer saline (PBS) solution of pH 7.4. The PEGylated gold nanobipyramids were stored at 4 °C till further use.

Conjugation of gold nanobipyramids with anti-MUC1 aptamer

The conjugation of nanobipyramids with anti-MUC1 aptamer involves two steps, viz., (a) surface modification of nanobipyramids with capture oligonucleotides and (b) hybridization of capture oligonucleotides with Alexa-480-tagged anti-MUC1 aptamer sequence.

(a) Surface modification of nanobipyramids with capture oligonucleotides

The surface modification of nanobipyramids with capture oligonucleotides was performed using salt-aging approach. Briefly, the synthesized gold nanobipyramids were centrifuged at 8000 rpm for 10 min, and pellet was collected in a 2-mL centrifuge tube. To the above pellet, 100 µL of 2 mM CTAB solution was added and mixed gently with pipette for few seconds. To this, 50 µL of 2 mM mPEG-SH solution was added, and the mixing was continued for another few

seconds. Now, 835 µL of 1X phosphate buffer was added, and the tube was placed on shaker at 180 rpm for 30 min to check the stability of nanobipyramids. To the stable nanobipyramids solution, 15 µL of 10 µM capture oligonucleotide was added and placed on shaker for 16 h at room temperature.

After incubation, 2 M NaCl solution was added to the above mixture at an interval of 20 min with an increment of 0.05 M at each step till the final concentration of the solution was 1 M. After each addition of NaCl solution, sonication was performed for few seconds and placed on shaker. After achieving the final concentration of 1 M, the solution was aged for 24 h on shaker at room temperature. After aging, the unbound oligonucleotides were removed by spinning the solution at 12,000 rpm for 10 min and washed with resuspension buffer. The finally obtained capture oligonucleotide-nanobipyramids pellet was resuspended in 1 mL of resuspension buffer (1X PBS, 5% sucrose, 0.1% BSA, 0.01% Tween 20) and stored at 4 °C for further use.

(b) Hybridization of capture oligonucleotides with anti-MUC1 aptamer sequence

Firstly, both capture oligonucleotide-nanobipyramid conjugate solution and MUC1 aptamer solution were kept in a water bath at 70 °C, dark for 5 min to denature the secondary structures and cooled to room temperature naturally. Now, to 1 mL of capture oligonucleotide-nanobipyramid solution, 7.5 µL of 100 nM MUC1 aptamer was added and incubated for 30 min. The unhybridized aptamer sequences were removed by centrifuging at 12,000 rpm for 10 min and washed with resuspension buffer. Finally, the conjugate was again resuspended in 1 mL resuspension buffer and stored at 4 °C till further use.

Conjugation of gold nanobipyramids with anti-MUC1 antibody

The nanobipyramids were conjugated with anti-MUC1 antibody using carbodimide chemistry through EDC/NHS and cysteamine [15]. For the conjugation of antibody, the as-synthesized nanobipyramids were centrifuged for 10 min at 8000 rpm to remove the excess and unreacted reactants. To the pellet, 5 µL of 0.4 M cysteamine dihydrochloride and 10 mL of 16 mM HNO_3 were added. The mixture was aged for 30 min and centrifuged for 15 min at 8000 rpm. The pellet was dispersed in 1 mL of MilliQ. In a separate tube, 0.005% Tween 20 solution, 2 mM EDC, and 5 mM NHS were added, volumized to 1 mL and aged for 10 min. To this EDC/NHS mixture, 1.5 µL of 1 mg/mL of anti-MUC1 antibody was added and aged for at least 1 h at 4 °C. Now, EDC/NHS-modified antibody was added to 1 mL of cysteamine-modified gold nanobipyramids and aged for 1 h at 4 °C. After aging, the solution was centrifuged for 10 min at 8000 rpm to remove unbound antibodies, and the pellet was resuspended in 950 µL of sodium carbonate buffer and 50 µL of 2 mM mPEG-SH solution and incubated for overnight under gentle shaking. Followed by incubation, the solution was centrifuged for 10 min to remove unbound PEG. Finally, the pellet was resuspended in resuspension buffer and stored at 4 °C till further use.

Characterization of conjugation and unconjugated gold nanobipyramids

The as-synthesized gold nanobipyramids were characterized using CARY60 UV–Visible spectrophotometer (Agilent Technology) and transmission electron microscopy (TEM, H-7500, Hitachi). Surface modification with polyethylene glycol was confirmed with FTIR analysis using RZX (Perkin Elmer) Fourier-transform infrared spectrophotometer. The UV–Visible spectra of aptamer functionalized gold nanobipyramids were analyzed on CARY60 UV–Visible spectrophotometer (Agilent Technology) for determining their surface plasmon peaks. The surface functionalization of aptamer on nanobipyramids was confirmed by FTIR analysis using RZX (Perkin Elmer) Fourier transform infrared spectrophotometer. The internalization of aptamer-conjugated nanobipyramids was determined by fluorescence microscopy. The concentration of elemental gold of aptamer-conjugated nanobipyramids was determined using inductively coupled plasma mass spectroscopy (ICP-MS)

analysis (Element XR, Thermo Fisher Scientific). The conjugation of nanobipyramids with antibody was confirmed by using UV–Visible spectroscopy and fluorescence microscopy.

In vitro toxicity assessment of gold nanobipyramids

The toxicity of nanobipyramids was carried out on MCF7 breast cancer cell lines and HCT116 colon cancer cell lines using MTT assay. Biocompatibility studies were carried out on human red blood cells collected from healthy donors. The study was approved by the Institute Ethical committee (IEC No.: IEC/2019–20/05), and human blood samples were collected from volunteers after filling due consent form.

Cell culture

Human breast cancer cell line, MCF7, and human colon cancer cell line, HCT116, were procured from NCCS Pune, India. Both the cell lines were cultured in RPMI-1640 supplemented with 10% fetal bovine serum (FBS). The cells were maintained at 37 °C, 5% CO_2, and humidity to achieve optimal growth. The sub-culturing was carried out by trypsinization using 0.25% (w/v) trypsin/EDTA.

Effect of surface modification on the cytotoxicity and specific cell killing ability of nanobipyramids

To study the effect of surface modification of nanostructures on cytotoxicity towards MCF7 cell lines and HCT116 cell lines, the surface of nanobipyramids were modified with mPEG-SH, anti-MUC1 aptamer, and anti-MUC1 antibody. For this, the cells were seeded in 96 well plate at a density of 10^5 cells/mL in each well and incubated at 37 °C for 16 h. After achieving confluence, cells were incubated with different concentrations (25–200 µg/mL) of surface-modified/unmodified nanobipyramids for various time intervals (2, 4, 6, and 24 h) diluted in binding buffer (1X PBS, 4.5 g/Lt Glucose, 5 mM Magnesium chloride, 0.1 mg/mL Herring sperm DNA, 1 mg/mL BSA). Upon completion of treatment, nanobipyramid solution was removed, and cells were washed with wash buffer (1X PBS, 4.5 g/Lt glucose, 5 mM magnesium chloride). Now, the cell death was determined using MTT assay by incubating with MTT solution (100 µL of 0.5 mg/mL) for 4 h at 37 °C. The formazan crystals were dissolved by adding 150 µL of absolute DMSO followed by incubation at 37 °C for 15–20 min. Finally, the absorbance was read at 570 nm. The percentage cytotoxicity was calculated using the following formula:

$$\% \text{ Cytotoxicity} = 100 - \left[\left(\frac{\text{Absorbance of treated sample at 570 nm}}{\text{Absorbance of untreated sample at 570 nm}}\right) \times 100\right]$$

Cellular uptake studies on MCF7 cell lines and HCT116 cell lines

Cellular uptake studies were carried out by quantifying the amount of nanobipyramids taken up by the cells using ICP-MS. The cells were seeded at a density of 1×10^6 cells/mL in a 12 well plate and incubated for 20–24 h. After achieving the confluence of 80–85%, the cells were treated with aptamer- and antibody-conjugated nanobipyramids at a concentration of 75 µg/mL, 125 µg/mL for 6 h. mPEG-SH-modified nanobipyramids were employed as control to calculate the percentage nonspecific internalization of nanostructures. Upon completion of incubation time, the medium was discarded, and cells were washed with 1X PBS. Later, cells were etched with 1 mL of etching solution (I_2/KI solution in the ratio of 0.34 mM/0.24 mM) for 3 min and washed thrice with 1X PBS. Finally, cells were processed for ICP-MS analysis by digesting the cells with aqua regia at 90 °C overnight to release gold ions from the intracellular nanostructures. The percentage cellular uptake of gold was calculated using the below formula:

$$\text{Percentage uptake of gold} = \frac{\text{Total ppb of gold determined by ICP} - \text{MS analysis within cells}}{\text{Total ppb of gold at the time of exposure with cells}} \times 100$$

The percentage specific cellular uptake of aptamer/antibody-conjugated nanostructures by MCF7 cell lines was calculated by using the following equation:

$$\text{Percentage Specific Cellular Uptake} = \frac{(\%\ \text{Cellular uptake by MCF7 cell lines} - \%\ \text{Cellular uptake by HCT116 cell lines})}{\%\ \text{Cellular uptake by MCF7 cell lines}} \times 100$$

Biocompatibility assessment on RBCs

The biocompatibility assessment of nanostructures was performed on human red blood cells (RBCs). The biocompatibility was determined by calculating percentage hemolysis after treating RBCs with aptamer- and antibody-conjugated nanobipyramids.

Quantification of hemolysis

The hemolysis was quantified by determining the ratio of hemoglobin released into plasma (plasma hemoglobin) to total hemoglobin. Briefly, fresh blood from a healthy donor was collected in EDTA vacutainer. To 1 mL of freshly drawn blood, 100 µL of various concentrations (50, 75, 100, and 125 µg/mL) of aptamer/antibody-conjugated nanobipyramids diluted in binding buffer was added and incubated for 4 h and 6 h at 37 °C. After incubation, the treated blood samples were centrifuged for 10 min at 4500 rpm. The upper plasma portion was carefully collected in a fresh tube and diluted with 0.01% sodium carbonate solution in 1:1 ratio. Finally, the absorbance was noted at 415 nm, 380 nm, and 450 nm.

The plasma hemoglobin was calculated by applying the following equation.

$$\text{Plasma hemoglobin(mg/dL)} = \frac{\left(\left(2 \times A_{415}\right) - \left(A_{380} + A_{450}\right) \times\ 1000 \times\ \text{Dilution factor}\right)}{E \times 1.655}$$

where $E = 79.46$, which was the value of molar absorptivity of oxyhemoglobin that has maximum absorption at 450 nm; the constant value 1.655 was fractioned to minimize the interference raised due to the turbidity of plasma.

The percentage hemolysis was calculated using the following equation:

$$\text{Percentage Hemolysis} = \left(\frac{\text{Plasma hemoglobin of the treated sample}}{\text{Total hemoglobin of the blood}}\right) \times 100$$

Measurement of photothermal conversion properties

Photothermal conversion performance of nanobipyramids was measured by irradiating the solution of nanobipyramids to a continuous wave, solid state laser diode of wavelength, 808 nm (U-LD-80xxSeries Laser Diode, Union Optronics Corporation, Taiwan). Briefly, 150 µL of different concentrations (25, 50, 75, 100, 125, 150, 175, and 200 µg/mL) of nanostructure solution was taken in a 96-well plate, and the solution was exposed to laser with a power density of 1 W/cm^2 for 15 min. The temperature of the solution was measured by inserting a digital thermometer integrated with thermocouple probe into the solution. The change in temperature was recorded for every 1 min. Pure water was used as a control to calculate photothermal conversion efficiency. To study the effect of surface modification on photothermal conversion properties, the surface of both nanobipyramids was modified with mPEG-SH, anti-MUC1 aptamer, and anti-MUC1 antibody, and the photothermal conversion properties were measured as discussed above.

Photostability studies

The photostability of nanobipyramids was investigated by irradiating the nanobipyramids' solution of concentration 200 µg/mL to laser for 15 min (LASER ON) followed by natural cooling to room temperature for 15 min without laser irradiation (LASER OFF). This process was repeated for 9 cycles.

In vitro photoablation studies on cell lines

The in vitro photothermal studies were carried out on MCF7 cell lines and HCT116 cell lines by treating them with aptamer/antibody-conjugated nanobipyramids. To carry out this study, the cells were trypsinized and seeded in a 96 well plate, followed by incubation at 37 °C for 16–18 h. After achieving the confluence, the medium was discarded and washed with 1X PBS or incomplete culture medium to remove loosely adhered cells. The cells were treated with different concentrations (50, 75, 100, and 125 µg/mL) of aptamer/antibody-conjugated nanobipyramids for 6 h diluted with binding buffer. Followed by the treatment, nanobipyramid solution was removed and cells were washed with wash buffer. Finally, cells were again suspended in wash buffer, exposed to laser for 15 min, and incubated for at least 3 h. After the completion of incubation, the cell damage was assessed by using MTT assay. For this, 100 µL of 0.5 mg/mL of MTT dye solution was added to the laser irradiated cells and incubated for 4 h at 37 °C. The formazan crystals were dissolved in 150 µL of absolute DMSO and incubated for 15–20 min at 37 °C. Finally, the absorbance was read at 570 nm. The percentage cytotoxicity was calculated using the formula

$$\% \text{ Cytotoxicity} = 100 - \left[\left(\frac{\text{Absorbance of treated sample at 570 nm}}{\text{Absorbance of untreated sample at 570 nm}}\right) \times 100\right]$$

The percentage-specific targeted photoablation was calculated by applying the following equation:

$$\text{Percentage Specific photoablation towards MCF7 cell lines} = \frac{\left(\begin{array}{l}\%\text{ Cell death of nanostructures treated MCF7 cell lines upon laser exposure}-\\ \%\text{ Cell death of nanostructures treated HCT116 cell lines upon laser exposure}\end{array}\right)}{\%\text{ Cell death of nanostructures treated MCF7 cell lines upon laser exposure}} \times 100$$

Statistical analysis

All the assays were repeated thrice in duplicate each time, and then, the mean ± standard deviation was calculated. The statistical difference between different groups was determined by applying two-way ANOVA analysis of variance by using Prism7 software. The difference was indicated as p value, and $p < 0.001$ was considered to be statistically significant.

Results and discussion

Synthesis and characterization of gold nanobipyramids

Gold nanobipyramids were synthesized using CTAC seed-mediated two-step synthesis approach. The UV–Visible spectra of gold nanobipyramids (Fig. 1a) showed two distinct peaks, one in visible region termed as Transverse Plasmon Resonance Peak (TSPR) and the other in NIR region termed as Longitudinal Plasmon Resonance Peak (LSPR). TSPR and LSPR have their absorption maxima at 544 nm and 805 nm, respectively. TEM micrographs (Fig. 1b) and size distribution histograms (Fig. 1c, d) showed that the as-synthesized gold nanobipyramids possess an average length of 71.73 nm with SD of 7.9 nm and width of 27.7 nm with SD of 3.09 nm. The average aspect ratio was 2.5. Further, the percentage of nanobipyramids among all other shaped nanoparticles produced during synthesis was 85.4%.

Surface modification of gold nanobipyramids with mPEG-SH

Gold nanobipyramids were surface functionalized with mPEG-SH via standard gold-thiol chemistry.

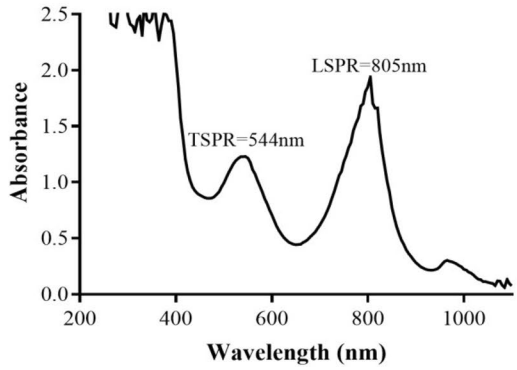
Absorbance
Wavelength (nm)
TSPR=544nm
LSPR=805nm

(a)

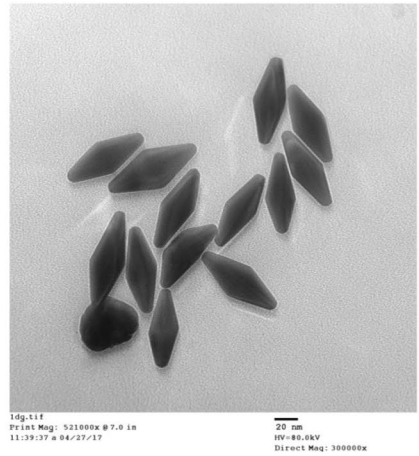
1dg.tif
Print Mag: 521000x @ 7.0 in
11:39:37 a 04/27/17
20 nm
HV=80.0kV
Direct Mag: 300000x

(b)

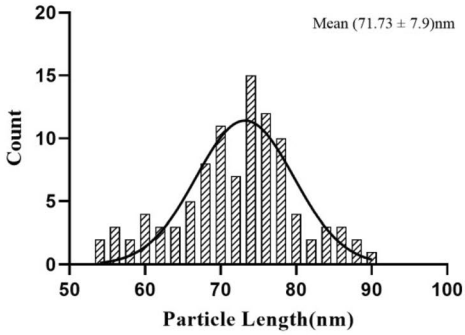
Mean (71.73 ± 7.9)nm
Count
Particle Length(nm)

(c)

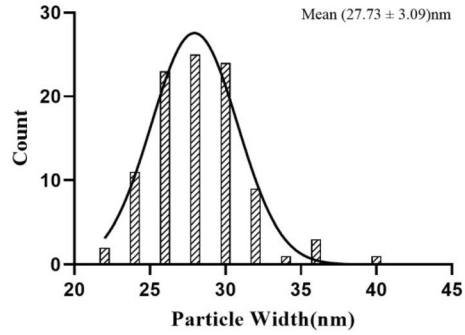
Mean (27.73 ± 3.09)nm
Count
Particle Width(nm)

(d)

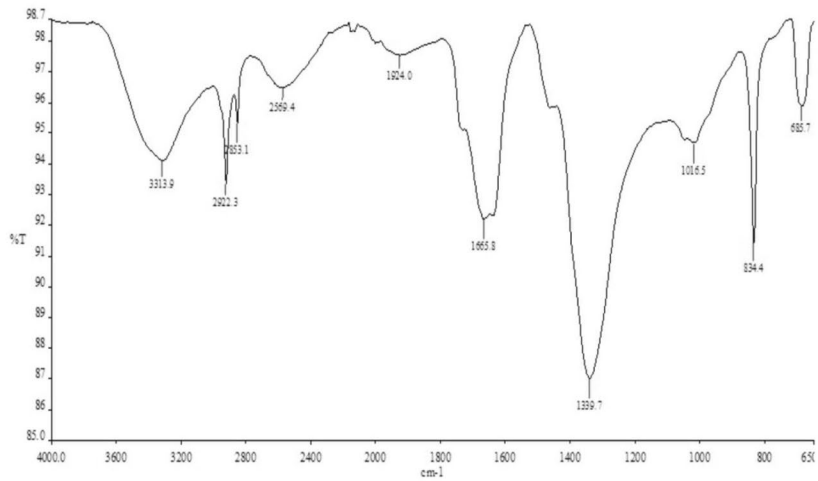
%T
cm-1
3313.9
2922.3
2853.1
2359.4
1924.0
1665.8
1399.7
1016.5
834.4
685.7

(e)

◂**Fig. 1** **a** UV–Visible spectrum of as synthesized nanobipyramids; **b** TEM micrograph of nanobipyramids; **c**, **d** size distribution graphs of gold nanobipyramids; **e** FTIR spectrum of PEGylated nanobipyramids

Introduction of PEG on surface of nanobipyramids was confirmed through FTIR analysis (Fig. 1e). The peak at 3316 cm^{-1} was due to O–H stretching in water molecules. The peak at 2853 cm^{-1} corresponds to C-H stretching of PEG molecules. Similarly, the peak at 685 cm^{-1} was generated by ethers present between polymeric groups and SH of PEG molecules. The absence of peak at 2550 cm^{-1} (S–H bond) can be attributed to the Au–S interaction [16]. The peaks between 1200 and 1000 cm^{-1} were due to the stretching of C-O bonds present in PEG. These strong IR bands corresponding to the vibrations and stretching of various bonds in PEG molecule confirms the surface capping of nanobipyramids with PEG.

Conjugation of gold nanostructures with MUC1 aptamer

Conjugation of nanobipyramids with MUC1 aptamer was achieved by employing two-step-mediated approach. In the first step, single-stranded DNA capture oligonucleotides of length 24 bases were loaded over the surface of nanobipyramids via standard gold-thiol chemistry and salt aging method. UV–Visible spectroscopic analysis of nanobipyramids-capture oligonucleotide conjugates (Fig. 2a) shows the shift in LSPR from 799 to 805 nm after conjugation. Similarly, FTIR analysis (Figure S1) also shows the characteristic peaks at 1132 cm^{-1}, 1106 cm^{-1}, and 1268 cm^{-1} which corresponds to phosphodiester bonds and glycosidic bond. Furthermore, the peak at 700 cm^{-1} represents the presence of ethers in mPEG-SH. The peak corresponding to S–H bond at 2550 cm^{-1} was not observed which confirms the formation of Au–S bond between thiolated aptamer and gold nanobipyramids. Thus, both UV–Visible spectra and FTIR spectra confirms the loading of capture oligonucleotides over the surface of gold nanobipyramids.

Second step involves the hybridization of nanobipyramids-capture oligonucleotide conjugate with MUC1 aptamer which was confirmed by UV–Visible spectroscopy, FTIR analysis, and fluorescence microscopy. UV–Visible spectra of nanobipyramids-MUC1 aptamer conjugates (Fig. 2b) show clear shift in their LSPR from 810 to 824 nm after hybridization. An FTIR spectrum of nanobipyramid-MUC1 aptamer conjugate (Figure S2) also confirms the hybridization by exhibiting the characteristic peaks at 1107 cm^{-1} and 1421 cm^{-1} which corresponds to phosphodiester bond and glycosidic bond, respectively. Furthermore, the peak at 1649 cm^{-1} attributes to the stretching vibrations of cytosine. Apart from UV–Visible spectra and FTIR spectra, conjugation was also confirmed by fluorescence microscopy. Fluorescence microscopic imaging of MCF7 cell lines treated with either aptamer-conjugated nanobipyramids or antibody-conjugated nanobipyramids was carried out at a concentration ranging from 5 to 200 µg/mL for different time intervals of 2, 4, 6, 8, and 10 h. However, for optimum visualization of fluorescence, 100 µg/mL, 150 µg/mL, and 2, 4, 6 h were chosen, and further studies were carried out at these parameters. The green fluorescence observed in MCF7 cells (Fig. 2c) confirms the conjugation of Alexa-480-tagged MUC1 aptamer over the surface of nanobipyramids. Moreover, the cells were counter stained with DAPI (blue) to visualize nucleus. This confirmed the successful loading of MUC1 aptamer over the surface of gold nanobipyramids.

The ICP-MS analysis of MUC1 aptamer-conjugated nanobipyramids determined the concentration of elemental gold in nanobipyramids as 254.034 ppm.

Surface modification of nanobipyramids with anti-MUC1 antibody

Nanobipyramids were conjugated with anti-MUC1 antibody using EDC/NHS chemistry. After the completion of conjugation process, conjugates were analyzed by UV–Visible spectroscopy and fluorescence microscopy. The UV–Visible spectroscopy analysis reported the shift in LSPR of nanobipyramids from 790 to 809 nm after conjugation (Fig. 3a).

For the fluorescence microscopy studies, MCF7 cell lines were treated with different concentrations (100, 150 µg/mL) of Alexa 480-tagged (green) anti-MUC1 antibody-conjugated nanobipyramids for various time intervals (4, 6 h). As seen in Fig. 3b, the green fluorescence observed in the cells confirms the conjugation of antibody over the surface of

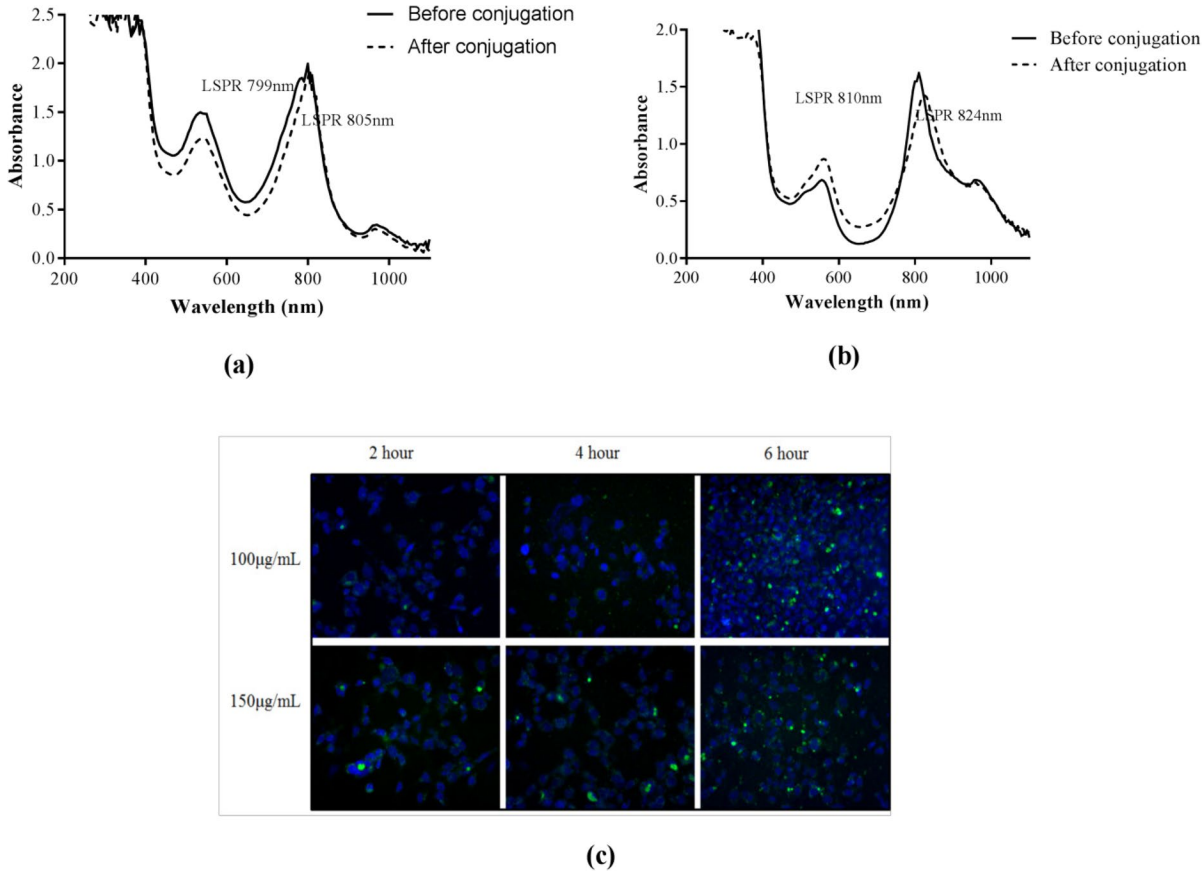

Fig. 2 **a** UV–Visible spectra of nanobipyramids before conjugation (LSPR: 799 nm) and after conjugation (LSPR: 805 nm) with capture oligonucleotide; **b** UV–Visible spectra of nanobipyramids before conjugation (LSPR: 810 nm) and after conjugation (LSPR: 824 nm) with anti-MUC1 aptamer; **c** fluorescence microscopic images of MCF7 cell lines treated with Alexa fluor 480-labeled anti-MUC1 aptamer-conjugated nanobipyramids (green) indicate the internalization of nanobipyramids and nuclei stained with DAPI (blue)

nanobipyramids. Also, determine the internalization of antibody-conjugated nanobipyramids and their localization in the cytoplasm, around the nucleus (blue).

Thus, the surface of gold nanobipyramids were modified by introducing different functional/targeting moieties, and its subsequent impact was investigated on two different cell lines (MCF7 and HCT116 cell lines) which vary in their surface expression of MUC1 tumor marker. The effect of surface modification and targeting moiety on cytotoxicity of gold nanobipyramids was determined using MTT assay, an in vitro cytotoxicity assay based on the activity of mitochondrial potential to reduce the dye into formazan crystals.

Assessment of percentage cell-specific killing ability of surface-modified and surface-unmodified gold nanobipyramids

To assess the percentage and specific cell killing ability towards cancerous cell lines, gold nanobipyramids were modified with anti-MUC1 aptamer or anti-MUC1 antibody. Naïve gold nanobipyramids and PEGylated nanobipyramids were used to assess nonspecific cell killing. Figure 4a–d shows the percentage cytotoxicity of surface modified gold nanobipyramids at 2 h, 4 h, 6 h, and 24 h, respectively, on MCF7 cell lines in comparison with unmodified nanobipyramids. The results showed a decrease in cytotoxicity (50% with aptamer conjugation and 16.8% with

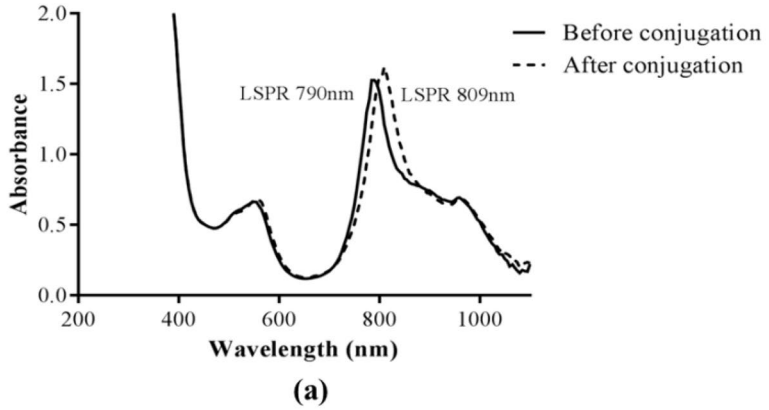

(a)

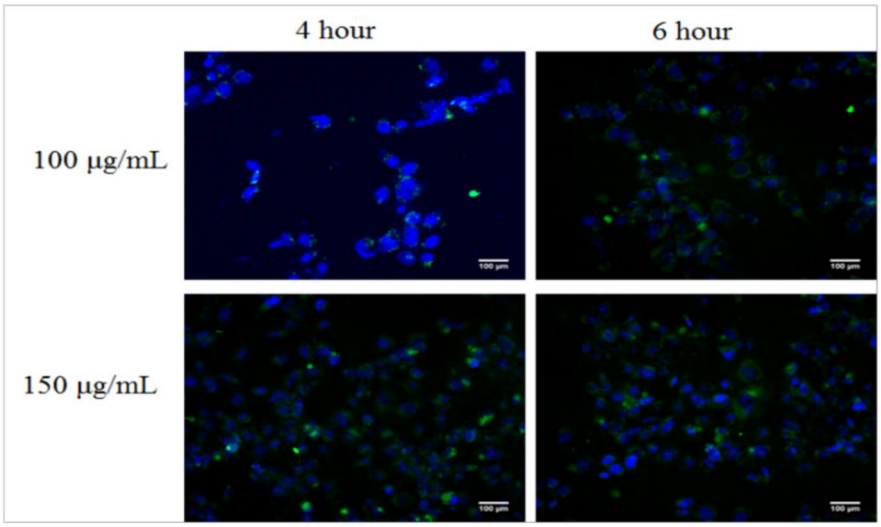

(b)

Fig. 3 **a** UV–Visible spectra of **a** nanobipyramids before conjugation (LSPR: 790 nm) and after conjugation (LSPR: 809 nm) with anti-MUC1 antibody; **b** fluorescence microscopic images of MCF7 cell lines treated with Alexa fluor 480-labeled antibody-conjugated nanobipyramids (green) indicate the internalization of nanobipyramids and nuclei stained with DAPI (blue)

antibody conjugation; treated with 200 µg/mL for 24 h) of nanobipyramids upon their surface modification. Similarly, Fig. 4e–h shows the percentage cytotoxicity of surface modified gold nanobipyramids at 2 h, 4 h, 6 h, and 24 h, respectively, on HCT116 cell lines. The cytotoxicity of nanobipyramids on HCT116 cell lines was observed to decrease (26% with aptamer conjugation and 9.4% with antibody conjugation; treated with 200 µg/mL for 24 h) after surface modification with either aptamer or antibody which was evident from the data.

To our surprise, it was observed that the toxicity of modified nanobipyramids towards MCF-7 cell lines was higher at 6-h compared to 24-h treatment for both aptamer- and antibody-modified nanobipyramids. Henceforth, all further analyses were carried out at 6-h treatment. From the above cytotoxicity data, IC50 values were calculated for aptamer- and antibody-conjugated gold nanobipyramids and found to be 110.788 µg/mL and 86.37 µg/mL, respectively. Thus, 125 µg/mL is determined to be the nearest concentration of IC50 value. Hence, further studies were carried out at this concentration.

Further comparative studies reported that naïve nanobipyramids and PEGylated nanobipyramids exhibited approximately similar level of cell killing on both MCF7 and HCT116 cell lines (Fig. 5a, b) at any concentration. This infers that unmodified nanobipyramids exhibited nonspecific cell killing because of their high cytotoxicity towards both the cell lines. However, conjugation with aptamer not only reduced the nonspecific cytotoxicity but also exhibited high specific killing towards MCF7 cell lines (41%) in comparison to antibody modified nanobipyramids (24%) (Fig. 5c, d).

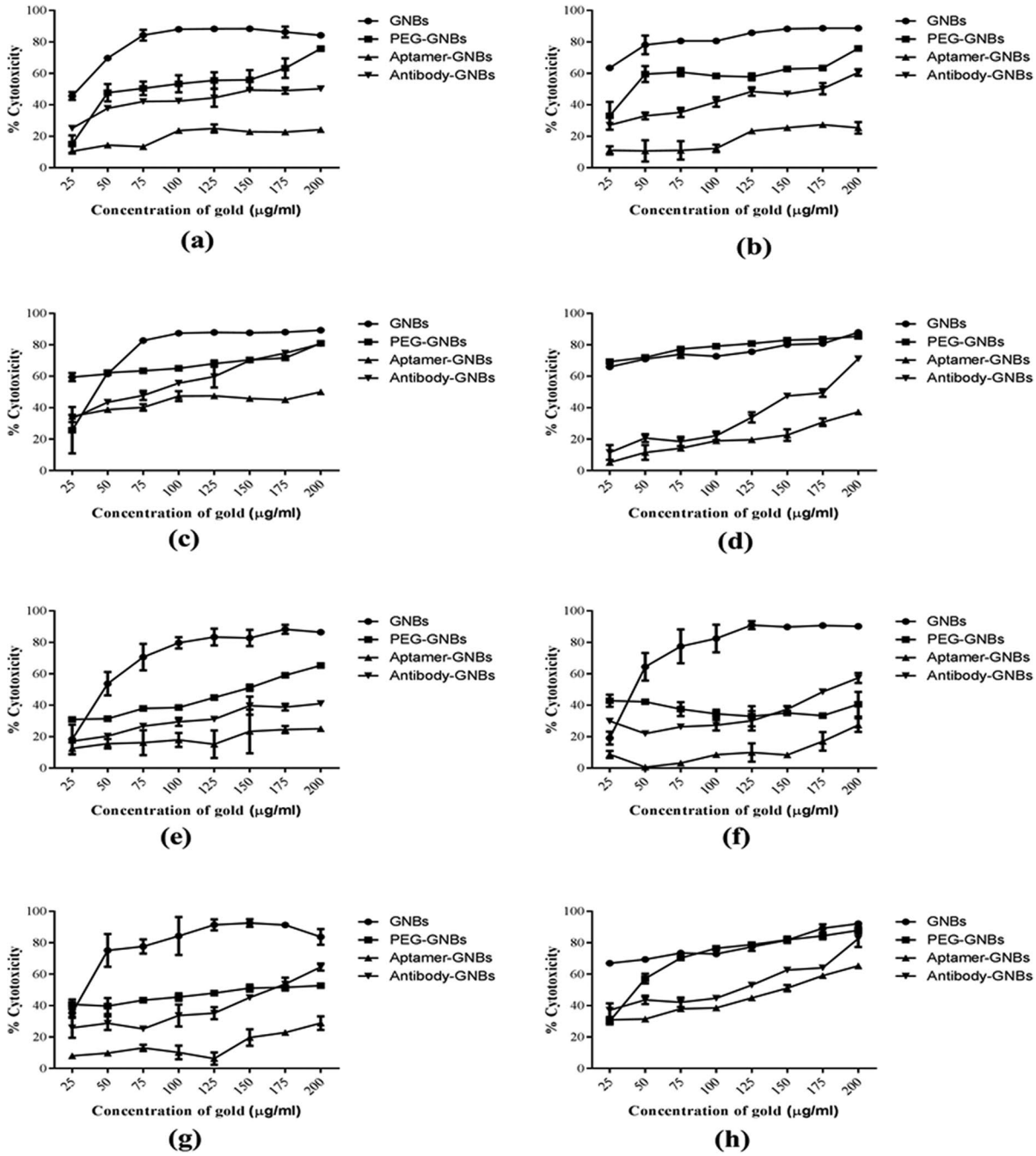

Fig. 4 In vitro toxicity profiling of nanobipyramids on **a**–**d** MCF7 cell lines and **e**–**h** HCT116 cell lines treated with naïve GNBs, PEG-GNBs, anti-MUC1 Aptamer-GNBs, and anti-MUC1 Antibody-GNBs for different time intervals: (**a**) 2 h; (**b**) 4 h; (**c**) 6 h; and (**d**) 24 h

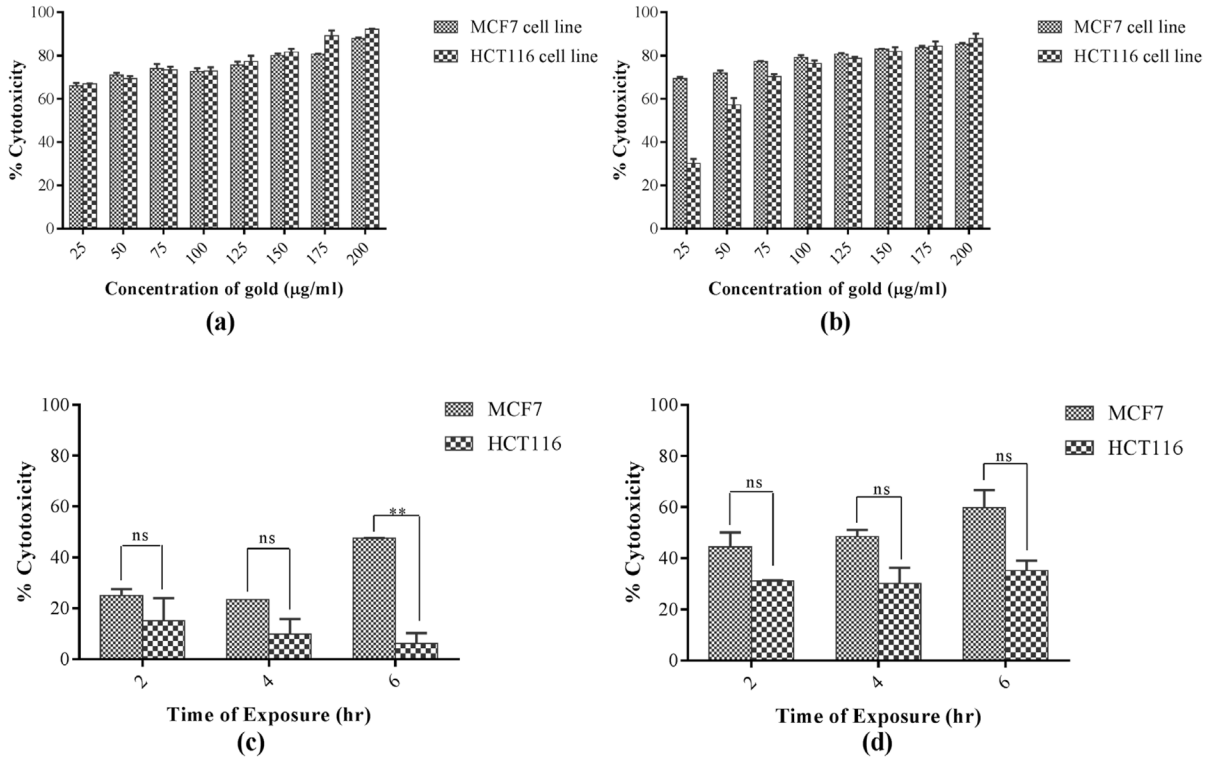

Fig. 5 Comparative toxicity profiling of **a** naïve nanobipyramids; **b** PEG modified nanobipyramids on MCF cell lines and HCT116 cell lines at different concentration exposed for 24 h. Comparative toxicity profiling of nanobipyramids modified with **c** anti-MUC1 aptamer; **d** anti-MUC1antibody on MCF7 cell lines w.r.t. HCT116 cell lines at different time intervals of exposure (statistical analysis compared with MCF7 cell lines at 125 µg/mL with HCT116 cell lines represents the p value, p = ns (non-significant), p = **(< 0.001))

Comparative analysis of targeting moiety towards killing cancerous cell lines

The effect of targeting moiety, i.e., aptamer or antibody on the ability of cell damage, was studied on MCF7 cell lines by treating the cells with surface functionalized nanobipyramids for different time intervals (2, 4, and 6 h) at a concentration of 125 µg/mL. The comparative effect of targeting moiety on cell killing ability of nanobipyramids on MCF7 cell lines is shown in Fig. 6a. At any exposure time antibody-conjugated nanobipyramids exhibited higher cell death than that of aptamer-conjugated nanobipyramids. After 2 h of exposure with aptamer-conjugated nanobipyramids, the cytotoxicity was observed to be 24.5%, whereas with antibody-conjugated nanobipyramids, it was observed to be 44%. Similarly, after 4 h of treatment, the cytotoxicity was 23% and 48% with aptamer-conjugated nanobipyramids and antibody-conjugated nanobipyramids, respectively. However, with the increase in time of exposure to 6 h, the difference between the cytotoxicity of aptamer-conjugated and antibody-conjugated nanobipyramids was decreased, i.e., 47% and 59%, respectively.

Figure 6b represents the comparative analysis of effect of targeting moiety on the cytotoxicity of nanobipyramids. Here, with HCT116 cell lines also, the cytotoxicity of antibody-conjugated nanobipyramids was increased with increase in exposure time, whereas reverse trend was observed with aptamer-conjugated nanobipyramids. The cytotoxicity of aptamer-conjugated nanobipyramids and antibody-conjugated nanobipyramids was observed to be ~ 6% and ~ 34%, respectively, after 6 h of exposure with HCT116 cell lines.

Specific toxicity of nanostructures on MCF7 cell lines w.r.t. HCT116 cell lines

Based on the above cytotoxicity data, the specific toxicity of aptamer/antibody-functionalized

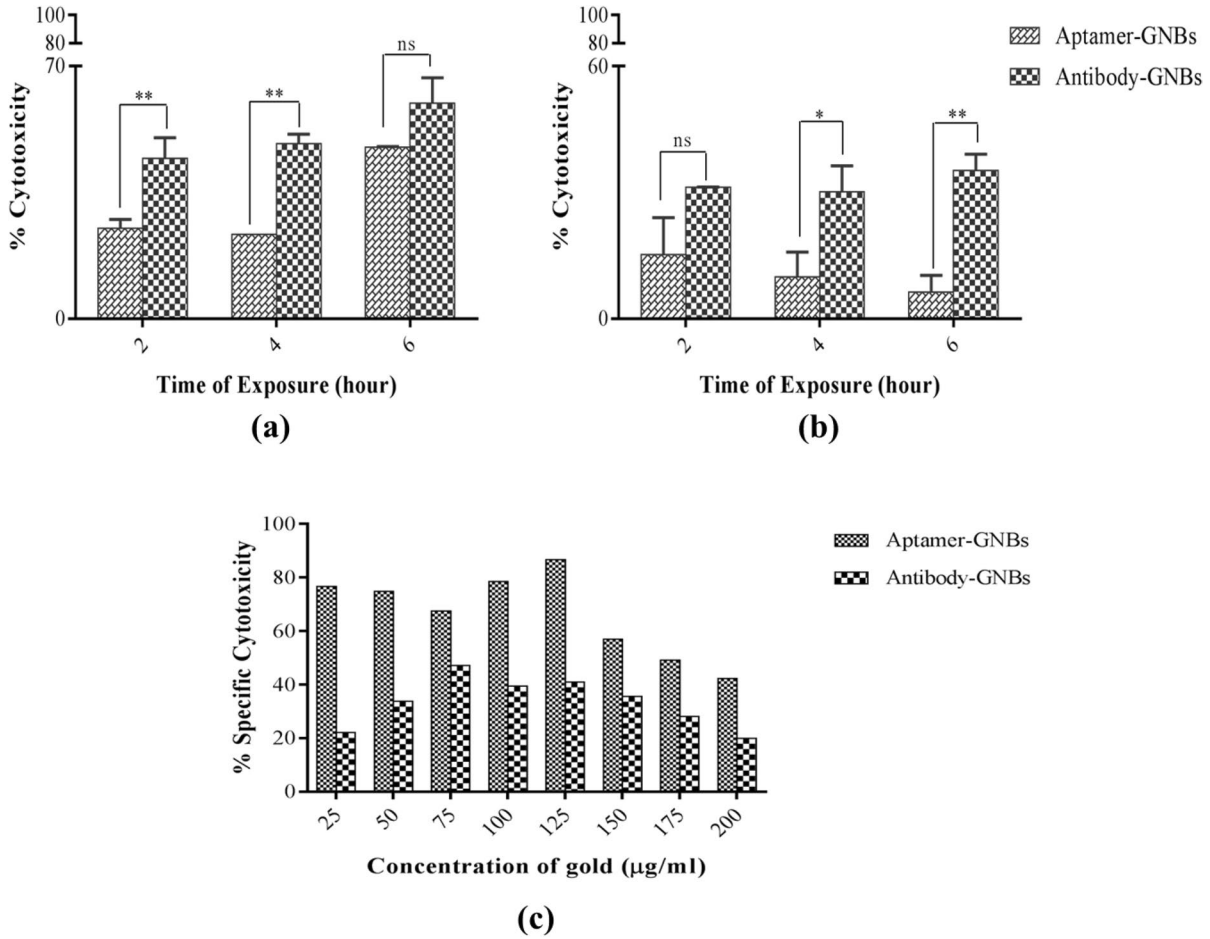

Fig. 6 Histograms depicting the effect of targeting moiety on nanobipyramid's surface towards killing **a** MCF7 cell lines and **b** HCT116 cell lines at different time intervals of exposure at 125 µg/mL. Statistical analysis compared within the group represents the p value, $p = ***$ (< 0.0001), $p = **$ (< 0.001), $p = *$ (< 0.01), $p =$ ns (non-significant); **c** histograms depicting percentage specific cell killing (MCF7 cell lines w.r.t. HCT116 cell lines) by anti-MUC1 aptamer- and anti-MUC1 antibody-conjugated nanobipyramids on treated for 6 h

nanobipyramids on MCF7 cell lines w.r.t. HCT116 cell lines was calculated using the following formula:

$$\frac{(\%\text{Cytotoxicity of nanoconjugates on MCF7 cell lines} - \%\text{Cytotoxicity of nanoconjugates on HCT116 cell lines})}{\%\text{Cytotoxicity of nanoconjugates on MCF7 cell lines}} \times 100$$

The results showed that the specific cytotoxicity was decreased with increase in the concentration of nanobipyramids functionalized either with aptamer or antibody. Aptamer-conjugated nanobipyramids showed greater specific cell death than antibody-conjugated nanobipyramids at lower concentrations (Fig. 6c).

Cellular uptake studies of nanobipyramids on MCF7 cell lines and HCT116 cell lines

Cellular internalization of surface-modified gold nanobipyramids was investigated by quantifying the percentage of elemental gold content within the cells by using ICP-MS analysis. The studies were carried out at 6-h exposure with 75 µg/mL and 125 µg/mL of aptamer and antibody functionalized nanobipyramids. PEGylated nanobipyramids were used as control to

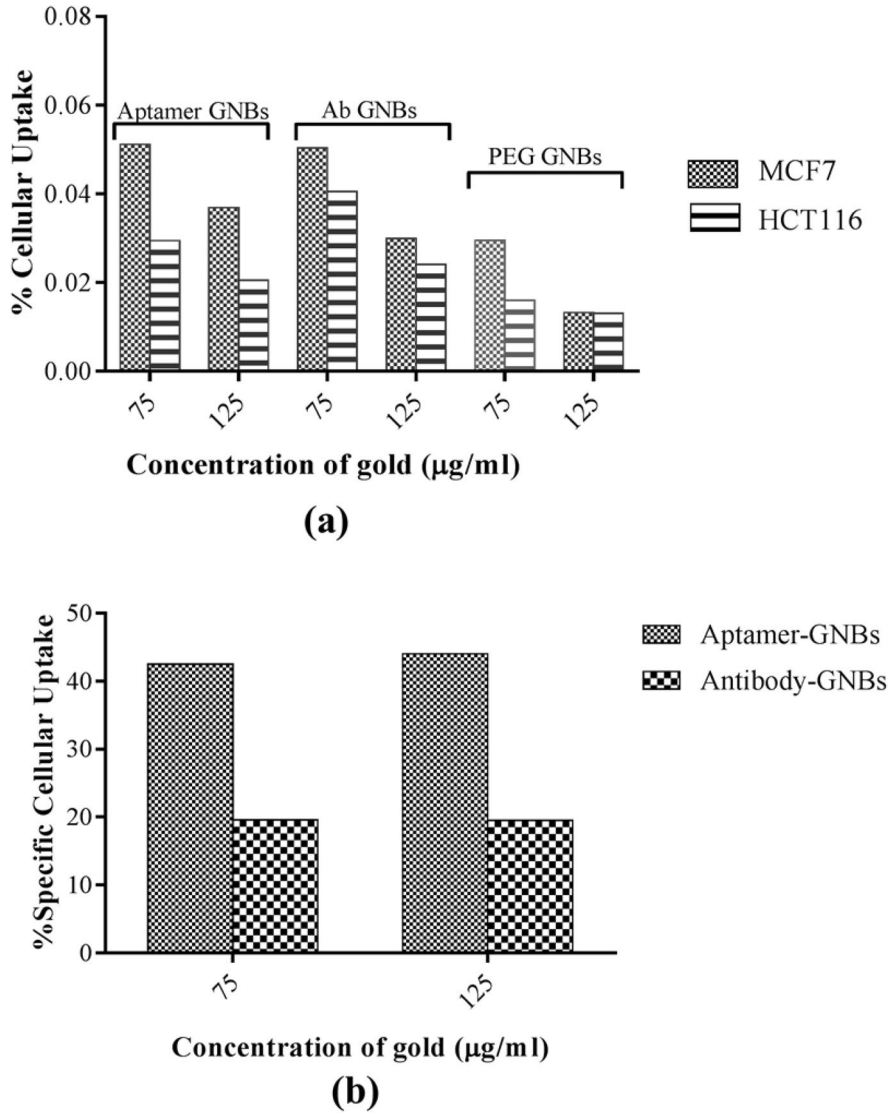

Fig. 7 **a** Percentage cellular uptake of targeting moiety functionalized nanobipyramids by MCF7 cell lines and HCT116 cell lines analyzed by ICP-MS; **b** percentage-specific cellular uptake of aptamer- and antibody-conjugated nanobipyramids by MCF7 cell lines w.r.t. HCT116 cell lines

subtract the nonspecific internalization of nanostructures. The percentage of intracellular elemental gold as quantified by ICP-MS showed the decrease in internalization with increase in concentration, irrespective of nature of targeting moiety. In the case of aptamer-conjugated nanobipyramids (Fig. 7a), at 75 µg/mL, the percentage intracellular gold was calculated to be 0.0511% for MCF7 cell lines and 0.0294% for HCT116 cell lines, whereas, at 125 µg/mL, the percentage intracellular gold was decreased to 0.0369% for MCF7 cell lines and 0.0204% for HCT116 cell lines. Similarly, in the case of antibody-conjugated nanobipyramids, the percentage intracellular gold was determined to be 0.0503% and 0.0404% for MCF7 cell lines and HCT116 cell lines at 75 µg/mL, respectively. At 125 µg/mL concentration, 0.0299% and 0.0241% of intracellular gold from antibody-conjugated nanobipyramids was determined in MCF7 cell lines and HCT116 cell lines, respectively.

PEGylated nanobipyramids showed nonspecific internalization in both the cell lines which was evident from the percentage intracellular gold determined from ICP-MS data (0.029% and 0.015% for MCF7 cell lines and HCT116 cell lines at 75 µg/mL,

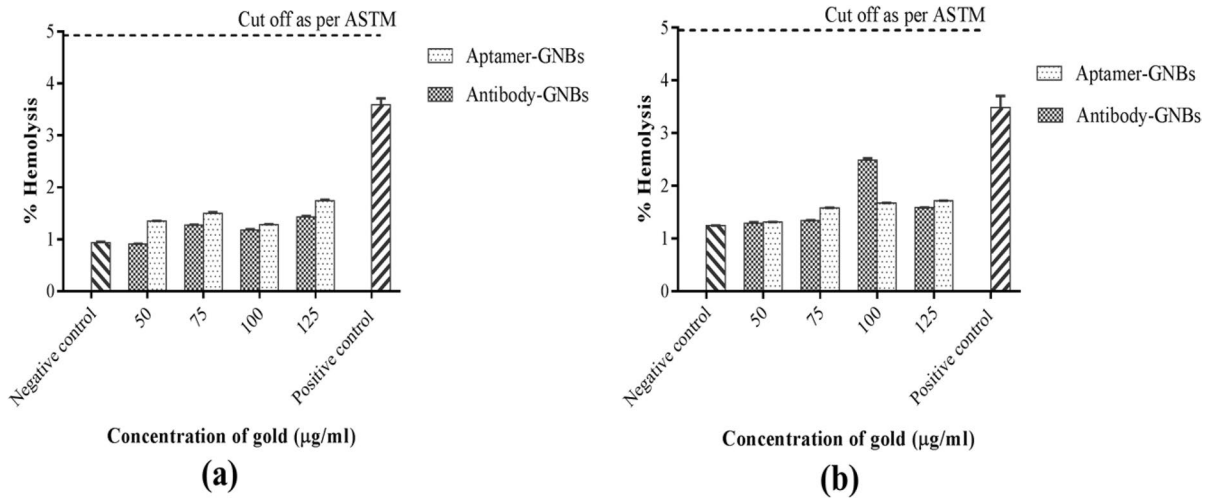

Fig. 8 Hemolytic profiling of target moiety functionalized nanobipyramids at a time interval of **a** 4 h and **b** 6 h

respectively; 0.013% for both the cell lines at 125 μg/mL).

Further, percentage-specific cellular uptake of nanostructures by MCF7 cell lines w.r.t. HCT116 cell lines (Fig. 7b) was calculated using ICP-MS analysis data by employing percentage specific cellular uptake equation. These results showed that aptamer-conjugated nanobipyramids were more internalized than antibody-conjugated nanobipyramids. The results of ICP-MS data were in accordance with specific cytotoxicity data which reported that the aptamer-conjugated nanobipyramids exhibited greater and specific cytotoxicity towards MCF7 cell lines.

Biocompatibility studies on RBCs

The biocompatibility studies were carried out by quantifying the percentage hemolysis of RBCs. Further, the percentage hemolysis was quantified by estimating the hemoglobin released form the lysed RBCs into plasma at 380 nm, 415 nm, and 450 nm after the treatment of freshly drawn blood with different concentrations of surface-modified nanobipyramids for 4 h and 6 h. Figure 8a, b shows the hemolytic profile of surface modified nanobipyramids at 4 h and 6 h of exposure time, respectively. The data showed that nanobipyramids caused hemolysis of RBCs with increase in concentration and time of exposure. However, percentage hemolysis was less than 2% at any concentration, time of exposure, and with either of the surface-modified nanobipyramids. Furthermore, there was no significant change in percentage hemolysis of RBCs as compared with negative control. These results were also in accordance with ASTM (American Standards for Testing and Materials) reference which says that percentage hemolysis > 5 after balancing the values of negative control was considered as hemolytic.

Measurement of photothermal properties of gold nanobipyramids

The photothermal conversion efficacy was calculated by irradiating different concentrations of nanobipyramids solution with 808-nm continuous wave laser of power density 1 W/cm^2 for 15 min, and then, the laser was turned off. The spot of the laser was adjusted to cover the whole sample. Pure water was used as a negative control. The change in temperature was recorded using thermocouple inserted into solution. The change in temperature of pure water upon laser irradiation was observed to be 3.3 °C. With increase in concentration of nanobipyramids from 25 to 200 μg/mL, the change in temperature was recorded to be 6.3 to 17.1 °C within 15 min (Fig. 9a). This indicates that nanobipyramids can efficiently convert the laser energy at 808-nm wavelength to thermal energy. Further, surface modification with mPEG-SH did not alter the conversion efficiency of nanobipyramids.

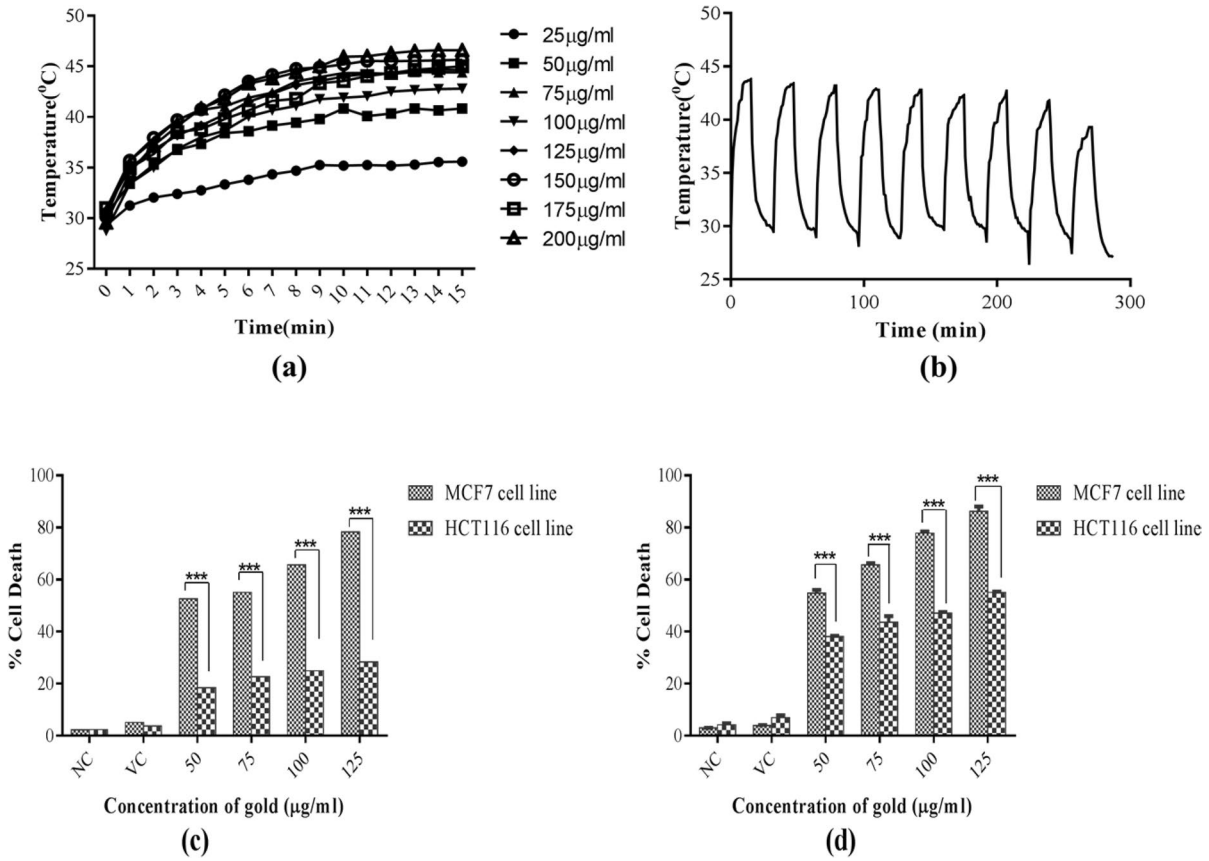

Fig. 9 **a** Temperature change of different concentrations of nanobipyramids solution upon 808-nm wavelength laser irradiation for 15 min; **b** stability of nanobipyramid (200 µg/mL) laser irradiation for 9 ON/OFF cycles; in vitro targeted photoablation studies on MCF7 and HCT116 cell lines irradiated with 808-nm laser for a period of 15 min. **c** Cells treated with anti-MUC1 Aptamer-GNBs for 6 h; **d** cells treated with anti-MUC1 antibody-GNBs for 6 h. NC: negative control; VC: vehicle control. Statistical analysis compared within the group represents the p value, $p = ***$ (< 0.0001), $p = **$ (< 0.001), $p = *$ (< 0.01), $p =$ ns (non-significant)

The photothermal conversion efficiency (η) of nanobipyramids was calculated using Roper's method as mentioned in the section. The η of nanobipyramids was calculated to be 14.59% (Supplementary file).

Photostability studies were carried out by irradiating the nanobipyramids with laser continuously for 9 ON/OFF cycles. Nanobipyramids (Fig. 9b) exhibited excellent photostability up to 9 cycles with slight variation in reaching the maximum temperature.

In vitro photoablation studies on MCF7 and HCT116 cell lines

In vitro photoablation studies were carried out by irradiating cells for 15 min with laser after exposing the cells with different concentrations (50, 75, 100, and 125 µg/mL) of aptamer/antibody-conjugated nanobipyramids for 6 h. Finally, the cell death after laser treatment was determined by MTT assay. Binding buffer was used as vehicle control and culture medium as negative control. In comparison to nanostructure-treated cells, only laser-treated cells showed negligible cell death. Aptamer-conjugated nanobipyramids showed 52%, 55%, 65%, and 77% death at concentrations of 50, 75, 100, and 125 µg/mL, respectively (Fig. 9c), whereas antibody-conjugated nanobipyramids showed 54%, 65%, 77.5%, and 85% of cell death at concentrations of 50, 75, 100, and 125 µg/mL, respectively (Fig. 9d) on MCF7 cell lines. From the above data, it was observed that

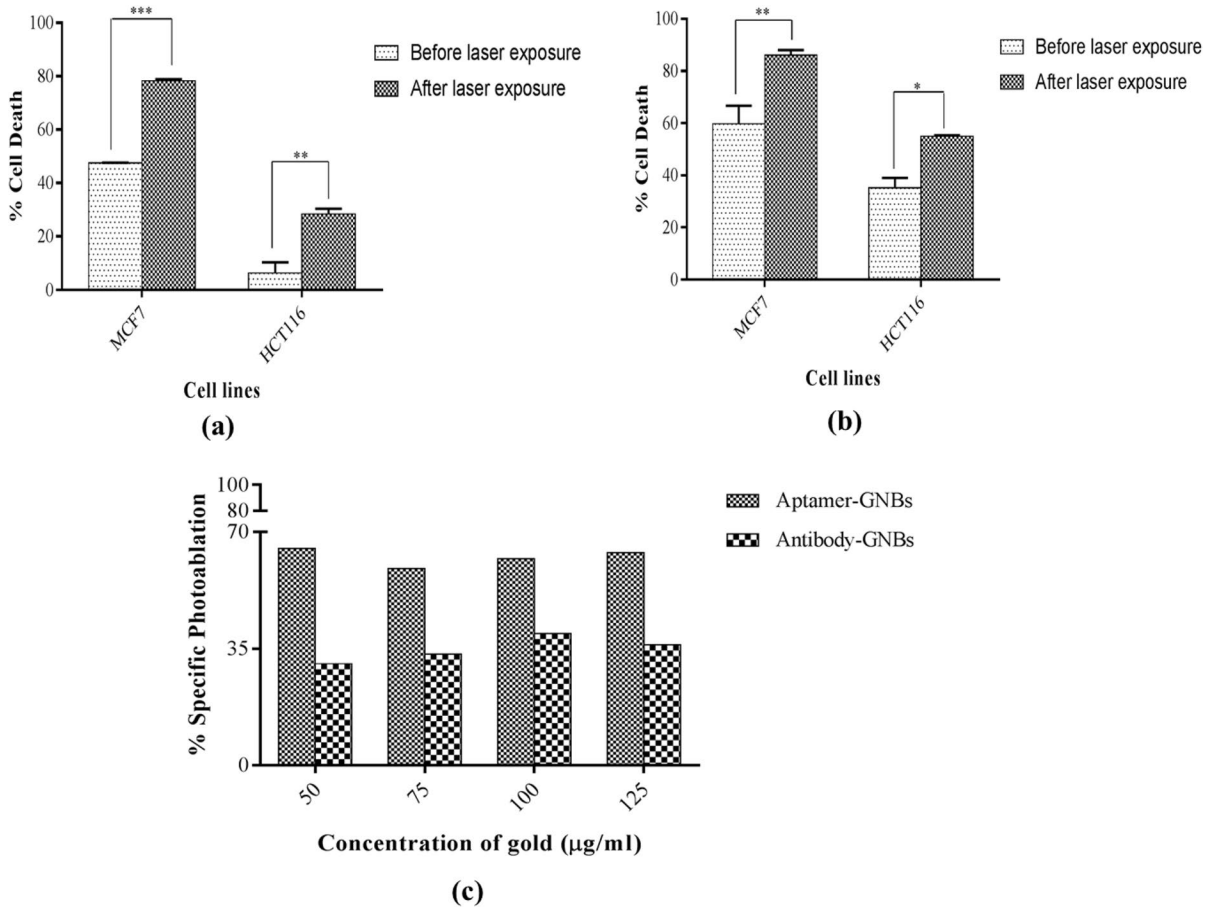

Fig. 10 Histograms depicting % cell death of **a** aptamer-conjugated nanobipyramids and **b** antibody-conjugated nanobipyramids on MCF7 cell lines and HCT116 cell lines before and after laser irradiation for 15 min; **c** histograms depicting % specific photoablation of aptamer and antibody against MUC1-conjugated nanobipyramids on MCF7 cell lines w.r.t. HCT116 cell lines treated for 6 h and laser irradiation for 15 min. Statistical analysis compared within the group represents the *p* value, $p = ***$ (< 0.0001), $p = **$ (< 0.001), $p =$ ns (non-significant)

aptamer-conjugated nanobipyramids exhibited more specific photoablation effect on MCF7 cell lines in comparison to antibody-conjugated nanobipyramids. Moreover, this data was in line with percentage cell death of MCF7 cell lines before and after laser irradiation (Fig. 10a, b).

Specifically targeted photoablation studies

To determine the percentage-specific cell death upon photoablation of MCF7 cell lines w.r.t. HCT116 cell lines, the above data of photoablation studies on cell lines was reanalyzed using the formula. As observed in specific cytotoxicity of nanobipyramids, similar trend was observed for specific cell death for photoablation studies. In detail, aptamer-conjugated nanobipyramids showed greater specific photoablation (63%) in comparison to antibody-conjugated nanobipyramids (36%) (Fig. 10c). Furthermore, aptamer-conjugated nanobipyramids caused greater specific cell death of MCF7 cell lines both before and after photoablation in comparison to HCT116 cell lines (Fig. 10a) than that of antibody-conjugated nanobipyramids (Fig. 10b).

The physicochemical properties of nanostructures determine their toxicity and light absorption properties. Hence, here in the present study, the effect of surface modification with different targeting moieties on cytotoxicity and photoablation effect of gold nanobipyramids was explored on MCF7 cell

lines and HCT116 cell lines. The cytotoxicity studies were carried out using in vitro MTT assay and correlated with ICP-MS data. Naive nanobipyramids exhibited linear increase in cytotoxicity with concentration and time of exposure towards both the cell lines. Furthermore, naïve nanobipyramids exhibited higher cytotoxicity (> 80%) on both the cell lines even at lower concentration and shorter exposure time of 2 h. There is a relative dearth of direct cytotoxicity assessment of gold nanobipyramids or their correlation with other gold nanoparticles. However, the results of the study were in accordance with previous studies conducted on other gold nanostructures. For instance, studies conducted by Carnovale group [17] and Tarantola group [18] demonstrated that gold nanostructures stabilized by CTAB exhibited greater cytotoxicity on cells. Further, few studies reported that nanoparticles with small core size such as nanospheres, nanorods, and nanobipyramids exhibit comparatively higher cytotoxicity than that of nanoparticles with larger core size (nanostars, nanoflowers) [19, 20]. Hence, to reduce cytotoxicity and increase stability, nanobipyramids were surface functionalized with PEG [21, 22], and the cytotoxicity was assessed. The cytotoxicity of PEGylated nanobipyramids was found to be greater than 40% at any concentration and shorter exposure time on both the cell lines. Though PEGylation decreased the cytotoxicity of nanobipyramids, yet it was greater than 60% at 24 h of exposure. Many studies reported negligible cytotoxicity of gold nanostructures upon surface functionalization with PEG [22, 23]. However, toxicity, cellular uptake, and biodistribution of PEGylated gold nanostructures are multifactorial and depend on molecular weight of PEG [21], terminal group on PEG [23], loading density on nanostructures, and conformation [24]. For instance, the study conducted by Uz et al. (2016) showed that gold nanoparticles coated with PEG caused DNA damage and led to cell cycle arrest irrespective of loading density of PEG on CaCo2 and PC3 cancer cell lines. Furthermore, the study also demonstrated that PEGylated gold nanoparticles did not cause any DNA damage in 3T3 normal cell lines at a loading density of ~ 0.65 chains/nm^2, whereas severe DNA damage was observed below and above this density [25].

Next, gold nanobipyramids were surface modified with anti-MUC1 aptamer and anti-MUC1 antibody to enhance the targeted delivery and further reduce the cytotoxicity. Irrespective of the nature of targeting moiety, cytotoxicity was greatly reduced at any concentration and exposure time w.r.t. naïve or PEG-modified nanobipyramids. However, cytotoxicity was higher at 6-h treatment compared to 24-h treatments, and the % of intracellular gold determined using ICP-MS at 6-h treatment was also higher at 75 µg/mL concentration compared to 125 µg/mL. It indicates that the cellular uptake decreases with higher concentration of aptamer/antibody-functionalized nanobipyramids. Enea et al. (2019) [26] also reported a similar decrease in cellular uptake with increase in concentration of gold nanoparticles which was attributed to agglomeration and internalization mechanism of nanoparticles. It was demonstrated and hypothesized that at lower concentrations, most of the nanoparticles remain as single particles and so penetrate the plasma membrane via passive diffusion faster, whereas, at high concentrations, nanoparticles tend to aggregate, and so, cellular internalization occurs through endocytosis which is a time-taking process [27]. Hence, at lower concentrations, amount of accumulated nanoparticles within cells is more even for shorter exposure time periods (6 h) resulting in high cellular damage compared to longer exposure time (24 h). Furthermore, cells during logarithmic phase are more sensitive to xenobiotic compounds compared to cells at stationary phase [20].

It was observed that aptamer-conjugated nanobipyramids exhibited more specific killing of MCF7 cell lines compared to antibody-conjugated nanobipyramids (45%) at 125 µg/mL. This could be explained in context with ICP-MS data which showed higher internalization of aptamer-conjugated nanobipyramids than antibody-conjugated nanobipyramids in MCF-7 cell lines. Though there were no studies on direct comparison of effect of targeting moiety on specific killing of nanobipyramids, however, the individual studies w.r.t. other gold nanostructure are available. The results of present study were in accordance with the recent study conducted by Kadkhoda et al. [28] which reported the efficient specific damage of MUC1-positive cell lines by anti-MUC1 aptamer-modified PEGylated gold nanoparticles. Similarly, Mahlknecht et al. [29] compared the efficiency of DNA aptamer and antibody against HER2 marker and reported the greater ability of aptamer against antibody in reducing HER2-expressing tumor

growth in xenografted mice. The nonspecific internalization into HCT116 cell lines and their cell damage indicates that nanobipyramids were probably getting internalized by passive approach rather than receptor-mediated internalization. However, to establish this explanation, the mechanism of internalization and mechanism of cell killing may be investigated in futuristic studies.

The biocompatibility studies were carried out on human RBCs by determining percentage hemolysis. Both aptamer and antibody-conjugated nanobipyramids showed biocompatibility towards RBCs at higher concentration (125 µg/mL) and exposure time (4, 6 h). Furthermore, percentage hemolysis of either of the surface-modified nanobipyramids was below the limits of ASTM. These results were in accordance with other studies [30] which demonstrate that gold nanoparticles (20 µM) either coated or uncoated with plasma proteins caused no significant hemolysis at an exposure time of 4 h. Another study showed that surface modification of gold nanobipyramids with hyaluronic acid reduced the percentage hemolysis to below 1.2% from 60% (before surface modification) [11].

Later, photothermal conversion efficiency of nanobipyramids was calculated to be 14.59% and found to be photostable upto 9 cycles. Previous studies reported photothermal conversion efficiency of gold nanobipyramids about 71% [9], 40–97% based on excitation wavelength [31], and 42% [32] which was comparatively higher than that of the calculated value in the present study. The reason for low photothermal conversion efficiency might be due to the laser system chosen for the photothermal treatment. Inspite of low photothermal conversion efficiency, the change in temperature of the solution was recorded to be 14 °C and 17 °C at 125 µg/mL and 200 µg/mL, respectively, and temperature reached to 45 °C which is an optimum temperature to damage cancerous cells [33, 34]. Zhang and group [35] demonstrated the importance of optimum temperature and mechanism of cell damage for efficient photoablation of cancerous cells. The study reported that cell damage was inefficient (10.2% of apoptosis, 18.3% of necroptosis, and 17.6% of necrosis) at temperatures < 43 °C, whereas at 49 °C, necrosis was observed to be dominant, and at 46 °C, the cell death (35.1%) was due to necroptosis. Gold nanobipyramids exhibited excellent photostability upto 9 cycles which is comparable to data reported by previous studies [9, 36]. Finally, in vitro photoablation studies showed that nanobipyramids exhibited specific MCF7 cell death compared to HCT116 cell death before and after laser irradiation irrespective of targeting moiety. Photoablation studies conducted by Feng and group showed that 808-nm laser irradiation of folic acid-conjugated gold nanobipyramids reduced the cell viability to 6.44% [10]. With respect to targeting moiety, aptamer conjugation lead to more specific and higher cell death of MCF7 cell lines in comparison with antibody conjugation.

Conclusion

Gold nanobipyramids have been emerging as one of the cutting edge among other gold nanostructures because of their sharp edges and excellent light absorption capacity. Here, in the present study, photothermal properties of gold nanobipyramids and cell killing ability of anti-MUC1 aptamer/antibody-conjugated gold nanobipyramids were studied on breast cancer cell lines. The studies showed that naïve gold nanobipyramids and PEGylated nanobipyramids exhibited greater cell damage (< 80% even at lower exposure time intervals) towards both MCF7 cell lines and HCT116 cell lines. However, percentage cytotoxicity was significantly reduced after modification with aptamer and antibody. Comparative analysis showed that aptamer-conjugated nanobipyramids exhibited higher specific cell killing towards MCF7 cell lines compared to antibody-conjugated nanobipyramids which is line with cellular uptake studies. The photothermal conversion efficiency was calculated as 14.59% and showed photostability upto 9 cycles under 808-nm continuous wave laser irradiation. In vitro photo ablation studies revealed that aptamer-conjugated nanobipyramids were more specific in ablating MCF7 cell lines than that of antibody-conjugated nanobipyramids. However, further studies were to be carried out to investigate the detail mechanism underlying the cell death before and after laser irradiation and the effect of targeting moiety on cytotoxicity. The study could be advantageous in the development of specifically targeted photoablating gold nanostructures and their in vivo applications.

Acknowledgements The authors are thankful to SAIF-IIT Bombay, India, for providing TEM facility and ICP-MS facility and SAIF-Panjab Chandigarh, India, for providing FTIR

spectrophotometer facility. The authors are also thankful to Professor S. Krishna, Department of Biochemistry, Banaras Hindu University, India, for providing fluorescence microscope facility.

Declarations

Conflict of interest The authors declare no competing interests.

References

1. Hwang S, Nam J, Jung S, Song J, Doh H, Kim S (2014) Gold nanoparticle-mediated photothermal therapy: current status and future perspective. Nanomedicine (Lond) 9(13):2003–2022. https://doi.org/10.2217/nnm.14.147
2. Yang W, Liang H, Ma S, Wang D, Huang J (2019) Gold nanoparticle based photothermal therapy: development and application for effective cancer treatment. Sustain. Mater. Technol 22:e00109. https://doi.org/10.1016/j.susmat.2019.e00109
3. Liu Y, Crawford BM, Vo-Dinh T (2018) Gold nanoparticles-mediated photothermal therapy and immunotherapy. Immunotherapy 10(13):1175–1188. https://doi.org/10.2217/imt-2018-0029
4. Kou XS, Ni WH, Tsung CK, Chan K, Lin HQ, Stucky GD, Wang JF (2007) Growth of gold bipyramids with improved yields and their curvature-directed oxidation. Small 3:2103–2113. https://doi.org/10.1002/smll.200700379
5. Kou XS, Zhang SZ, Tsung CK, Yeung MH, Shi QH, Stucky GD, Sun LD, Wang JF, Yan CH (2006) Growth of gold nanorods and bipyramids using CTEAB surfactant. J Phys Chem B 110:16377–16383. https://doi.org/10.1021/jp0639086
6. Li Q, Zhuo XL, Li S, Ruan QF, Xu QH, Wang JF (2015) Production of monodisperse gold nanobipyramids with number percentages approaching 100% and evaluation of their plasmonic properties. Adv Opt Mater 3:801–812. https://doi.org/10.1002/adom.201400505
7. Feng J, Chen L, Xia Y, Xing J, Li Z, Qian Q, Wang Y, Wu A, Zeng L, Zhou Y (2017) Bioconjugation of gold nanobipyramids for SERS detection and targeted photothermal therapy in breast cancer. ACS Biomater Sci Eng 3(4):608–618. https://doi.org/10.1021/acsbiomaterials.7b00021
8. Li C, Mei E, Chen C, Li Y, Nugasur B, Hou L, Ding X, Hu M, Zhang Y, Su Z, Lin J, Yang Y, Huang P, Li Z (2020) Gold-nanobipyramid-based nanotheranostics for dual-modality imaging-guided phototherapy. ACS Appl Mater Interfaces 12(11):12541–12548. https://doi.org/10.1021/acsami.0c00112
9. Chow TH, Li N, Bai X, Zhuo X, Shao L, Wang J (2019) Gold nanobipyramids: an emerging and versatile type of plasmonic nanoparticles. Acc Chem Res 52(8):2136–2146. https://doi.org/10.1021/acs.accounts.9b00230
10. Wu X, Mu L, Sen Liang MC, Wang Y, She G, Shi W (2019) Bifunctional gold nanobipyramids for photothermal therapy and temperature monitoring. ACS Appl Bio Mater 2(6):2668–2675. https://doi.org/10.1021/acsabm.9b00344
11. Zhao S, Tian Y, Liu W, Su Y, Zhang Y, Teng Z, Zhao Y, Wang S, Lu G, Yu Z (2018) High and low molecular weight hyaluronic acid-coated gold nanobipyramids for photothermal therapy. RSC Adv 8:9023–9030. https://doi.org/10.1039/C7RA11667E
12. Deng X, Shao Z, Zhao Y (2021) Solutions to the drawbacks of photothermal and photodynamic cancer therapy. Adv Sci 8:2002504. https://doi.org/10.1002/advs.202002504
13. Qiao J, Li X, Qi L (2022) Fluorescent polymer-modified gold nanobipyramids for temperature sensing during photothermal therapy in living cells. Chinese Chem Lett 33(6):3193–3196. https://doi.org/10.1016/j.cclet.2021.12.070
14. Alves LN, Missailidis S, Lage CA, De Almeida CE (2019) Anti-MUC1 aptamer as carrier tool of the potential radiosensitizer 1, 10 phenanthroline in MCF-7 breast cancer cells. Anticancer Res 39(4):1859–1867. https://doi.org/10.21873/anticanres.13293
15. Guo YJ, Sun GM, Zhang L, Tang YJ, Luo JJ, Yang PH (2014) Multifunctional optical probe based on gold nanorods for detection and identification of cancer cells. Sens Actuators B 191:741–749. https://doi.org/10.1016/j.snb.2013.10.027
16. Devi S, Singh B, Paul AK, Tyagi S (2016) Highly sensitive and selective detection of trinitrotoluene using cysteine-capped gold nanoparticles. Anal Methods 8(22):4398–4405. https://doi.org/10.1039/C6AY01036A
17. Carnovale C, Bryant G, Shukla R, Bansal V (2019) Identifying trends in gold nanoparticle toxicity and uptake: size, shape, capping ligand, and biological corona. ACS Omega 4(1):242–256. https://doi.org/10.1021/acsomega.8b03227
18. Tarantola M, Pietuch A, Schneider D, Rother J, Sunnick E, Rosman C, Pierrat S, Sönnichsen C, Wegener J, Janshoff A (2011) Toxicity of gold-nanoparticles: synergistic effects of shape and surface functionalization on micromotility of epithelial cells. Nanotoxicology 5(2):254–268. https://doi.org/10.3109/17435390.2010.528847
19. Navyatha B, Nara S (2020) Comparative *in vitro* toxicity assessment of spiked anisotropic gold nanostructures. J Nanopart Res 22:116. https://doi.org/10.1007/s11051-020-04827-5
20. Wozniak A, Malankowska A, Nowaczyk G, Grzekowiak BF, Tunio K, Somski R, Medynska AZ, Jurga S (2017) Size and shape-dependent cytotoxicity profile of gold nanoparticles for biomedical applications. J Mater Sci Mater Med 28(6):92. https://doi.org/10.1007/s10856-017-5902-y
21. Liu Y, Shipton MK, Ryan J, Kaufman ED, Franzen S, Feldheim DL (2007) Synthesis, stability, and cellular internalization of gold nanoparticles containing mixed peptide–poly(ethylene glycol) monolayers. Anal Chem 79:2221–2229. https://doi.org/10.1021/ac061578f
22. Niidome T, Yamagata M, Okamoto Y, Akiyama Y, Takahashi H, Kawano T, Katayama Y, Niidome Y (2006) PEG-modified gold nanorods with a stealth character for *in vivo* applications. J Control Release 114:343–347. https://doi.org/10.1016/j.jconrel.2006.06.017
23. Reznickova A, Slavikova N, Kolska Z, Kolarova K, Belinova T, Hubalek Kalbacova M, Cieslar M, Svorcik V (2019) PEGylated gold nanoparticles: stability, cytotoxicity and antibacterial activity. Colloid Surfaces A 560:26–34. https://doi.org/10.1016/j.colsurfa.2018.09.083
24. Shi L, Zhang J, Zhao M, Tang S, Cheng X, Zhang W, Li W, Liu X, Peng H, Wang Q (2021) Effects of polyethylene

glycol on the surface of nanoparticles for targeted drug delivery. Nanoscale 13:10748–10764. https://doi.org/10.1039/D1NR02065J
25. Uz M, Bulmus V, Altinkaya SA (2016) The effect of PEG grafting density and hydrodynamic volume on gold nanoparticle-cell interactions: an investigation on cell cycle, apoptosis and DNA damage. Langmuir 32(23):5997–6009. https://doi.org/10.1021/acs.langmuir.6b01289
26 Enea M, Almeida MP, Eaton P, Silva DD, Pereira E, Soares ME, Bastos ML, Carmo H (2019) A multiparametric study of gold nanoparticles cytotoxicity, internalization and permeability using an in vitro model of blood-brain barrier. Influence of size, shape and capping agent. Nanotoxicology 13(7):990–1004. https://doi.org/10.1080/17435390.2019.1621398
27. Mustafa T, Watanabe F, Monroe W, Mahmood M, Xu Y, Saeed LM, Karmakar A, Casciano D, Ali S, Biris AS (2011) Impact of gold nanoparticle concentration on their cellular uptake by MC3T3-E1 mouse osteoblastic cells as analyzed by transmission electron microscopy. J Nanomedic Nanotechnol 2:6. https://doi.org/10.4172/2157-7439.1000118
28. Kadkhoda J, Aghanejad A, Safari B, Baar J, Rasta SH, Davaran S (2022) Aptamer-conjugated gold nanoparticles for targeted paclitaxel delivery and photothermal therapy in breast cancer. J Drug Deliv Sci Tec 67:102954. https://doi.org/10.1016/j.jddst.2021.102954
29. Mahlknecht G, Maron R, Mancini M, Schechter B, Sela M, Yarden Y (2013) Aptamer to ErbB-2/HER2 enhances degradation of the target and inhibits tumorigenic growth. Proc Natl Acad Sci U S A 110(20):8170–8175. https://doi.org/10.1073/pnas.1302594110
30. Aseichev AV, Azizova OA, Beckman EM, Skotnikova OI, Dudnik LB, Shcheglovitova ON, Sergienko VI (2014) Effects of gold nanoparticles on erythrocyte hemolysis. Bull Exp Biol Med 156:495–498. https://doi.org/10.1007/s10517-014-2383-6
31. Campu A, Craciun AM, Focsan M, Astilean S (2019) Assessment of the photothermal conversion efficiencies of tunable gold bipyramids under irradiation by two laser lines in a NIR biological window. Nanotechnology 30:405701. https://doi.org/10.1088/1361-6528/ab2d90
32. Liu Y, Li Z, Yin Z, Zhang H, Gao Y, Huo G, Wu A, Zeng L (2020) Amplified photoacoustic signal and enhanced photothermal conversion of polydopamine-coated gold nanobipyramids for phototheranostics and synergistic chemotherapy. ACS Appl Mater Interfaces 12(13):14866–14875. https://doi.org/10.1021/acsami.9b22979
33. Long S, Xu Y, Zhou F, Wang B, Yang Y, Fu Y, Du N, Li X (2019) Characteristics of temperature changes in photothermal therapy induced by combined application of indocyanine green and laser. Oncol Lett 17(4):3952–3959. https://doi.org/10.3892/ol.2019.10058
34. West CL, Doughty ACV, Liu K, Chen WR (2019) Monitoring tissue temperature during photothermal therapy for cancer. J BioX Res 2(4):159–168. https://doi.org/10.1097/jbr.0000000000000050
35. Zhang Y, Zhan X, Xiong J, Peng S, Huang W, Joshi R, Cai Y, Liu Y, Li R, Yuan K, Zhou N, Min W (2018) Temperature-dependent cell death patterns induced by functionalized gold nanoparticle photothermal therapy in melanoma cells. Sci Rep 8:8720. https://doi.org/10.1038/s41598-018-26978-1
36. Zhao S, Luo Y, Chang Z, Liu C, Li T, Gan L, Huang Y, Sun Q (2021) BSA-coated gold nanorods for NIR-II photothermal therapy. Nanoscale Res Lett 16(1):170. https://doi.org/10.1186/s11671-021-03627-7